R-matrix analysis of the *β* decays of ¹²N and ¹²B

S. Hyldegaard,[1,*] M. Alcorta,[2] B. Bastin,[3] M. J. G. Borge,[2] R. Boutami,[2] S. Brandenburg,[4] J. Büscher,[3] P. Dendooven,[4]
C. Aa. Diget,[5] P. Van Duppen,[3] T. Eronen,[6] S. P. Fox,[5] L. M. Fraile,[7] B. R. Fulton,[5] H. O. U. Fynbo,[1] J. Huikari,[6] M. Huyse,[3]
H. B. Jeppesen,[1] A. S. Jokinen,[6] B. Jonson,[8,9] K. Jungmann,[4] A. Kankainen,[6] O. S. Kirsebom,[1] M. Madurga,[2] I. Moore,[6]
A. Nieminen,[6] T. Nilsson,[8] G. Nyman,[8] G. J. G. Onderwater,[4] H. Penttilä,[6] K. Peräjärvi,[6] R. Raabe,[3] K. Riisager,[1]
S. Rinta-Antila,[6] A. Rogachevskiy,[4] A Saastamoinen,[6] M. Sohani,[4] O. Tengblad,[2] E. Traykov,[4] Y. Wang,[6]
K. Wilhelmsen,[8] H. W. Wilschut,[4] and J. Äystö[6]

[1]*Department of Physics and Astronomy, Aarhus University, DK-8000 Århus C, Denmark*
[2]*Instituto de Estructura de la Materia, CSIC, E-28006 Madrid, Spain*
[3]*Instituut voor Kern- en Stralingsfysica, K.U. Leuven, Celestijnenlaan 200D, B-3001 Leuven, Belgium*
[4]*Kernfysisch Versneller Instituut, University of Groningen, NL-9747 AA Groningen, The Netherlands*
[5]*Department of Physics, University of York, York YO10 5DD, United Kingdom*
[6]*Department of Physics, University of Jyväskylä, FIN-40014 Jyväskylä, Finland*
[7]*Grupo de Física Nuclear, Universidad Complutense, E-28040 Madrid, Spain*
[8]*Fundamental Physics, Chalmers University of Technology, S-412 96 Göteborg, Sweden*
[9]*PH Department, CERN, CH-1211 Genève 23, Switzerland*

The *β* decays of ¹²N and ¹²B have been studied at KVI and JYFL to resolve the composition of the broad and interfering 0^+ and 2^+ strengths in the triple-α continuum. For the first time a complete treatment of 3α decay is presented including all major breakup channels. A multilevel, many-channel *R*-matrix formalism has been developed for the complete description of the breakup in combination with the recently published separate analysis of angular correlations. We find that, in addition to the Hoyle state at 7.65 MeV, more than one 0^+ and 2^+ state is needed to reproduce the spectra. Broad 0_3^+ and 2_2^+ states are found between 10.5 and 12 MeV in this work. The presence of *β* strength up to the ¹²N *Q*-value window suggests the presence of additional 0^+ and 2^+ components in the ¹²C structure at energies above 12.7 MeV.

I. INTRODUCTION

Several open questions remain concerning the nature of the very broad resonances in ¹²C a few megaelectronvolts above the triple-α threshold. Only a broad state at 10.3 MeV has been included as a possible $T = 0$, 0^+ state in the current compilation for ¹²C [1]. Recently it has been confirmed that the dominating spin and parity of this component are in fact 0^+ [2–4]. Several experimental indications of 2^+ contributions in this region have been published [3–6]. These 2^+ states all overlap with the broad 0^+ component in the 10- to 12-MeV energy region, and a consistent picture has not yet emerged from the experiments.

The low-lying natural parity states in the triple-α continuum determine the stellar triple-α reaction rate. The Hoyle state at just 0.38 MeV above the triple-α threshold (Fig. 1) dominates this rate at temperatures relevant for helium burning in red giant stars, but 0^+ and 2^+ states at higher energy could play a role in the process in high-temperature environments [7]. The position of the 2^+ states above the Hoyle state is also a subject of major importance for the understanding of the cluster structure of ¹²C. Morinaga boldly suggested a linear chain structure of the Hoyle state [8] and later suggested the 10.3-MeV state to be a rotational excitation of the Hoyle state, therefore requiring a 2^+ assignment [9]. In modern microscopic cluster calculations

the connection between the 0^+ and the 2^+ states is suggested to be more complicated, with a stronger connection between the broad 0^+ component above the Hoyle state and the first 2^+ resonance [10].

β decay of ¹²N and ¹²B provides a clean probe of these broad structures. Selection rules in these *β* decays only allow decays to 0^+, 1^+, and 2^+ states, and the only 1^+ states below the *Q* value are the narrow 12.71- and 15.1-MeV states. Apart from the narrow 0^+ Hoyle peak at 7.654 MeV, the remaining *β*-decay spectrum therefore must consist of 0^+ and 2^+ components (see Fig. 1).

Here we report on measurements of the *β* decays of ¹²N and ¹²B using two complementary experimental methods. In the first experiment ¹²B and ¹²N beams were produced using the ISOL (isotope separation online) method and complete kinematics of the 3α breakup was measured by use of a setup of segmented detectors with large solid-angle coverage. This experiment is the latest in a series of measurements of ¹²B and ¹²N *β* decays using the ISOL method [2,7,11]. The second experiment was a high-statistics measurement of the total breakup energy spectra. This allows for measurement of very low-energy breakups, providing a spectrum including the Hoyle peak, 0.38 MeV above the threshold. Both experimental methods constitute major technical improvements compared to the early measurements of *β*-delayed 3α breakup of ¹²C in the 1950s and 1960s, where only the energies of single α particles were measured [12–14]. Several results from the present two experiments have already been published.
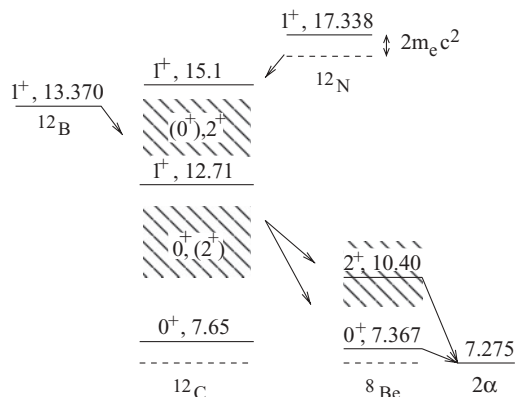
_____
*sgp@phys.au.dk

FIG. 1. β-delayed 3α breakup via ^{8}Be. Energies indicated as megaelectronvolts.

In Ref. [15] β-decay branching ratios are extracted, and, for narrow states, Gamow-Teller matrix elements deduced and compared to theory. More experimental details on this analysis for the ISOL experiment are given in Ref. [16]. These branching ratios do not distinguish between the subsequent decay of the ^{12}C states into 3α particles. This aspect is discussed separately in Ref. [17], where the full ^{12}C energy region populated in the ^{12}N/^{12}B decays is split into energy bins, and for each bin the breakup into 3α particles is analyzed. This breakup can proceed either via the 0^+ ground state in ^{8}Be or through higher energies in ^{8}Be (including direct breakup). The breakup through higher ^{8}Be energies is interesting for the purpose of separating 0^+ and 2^+ contributions because the sequences ^{12}C(2^+) $\rightarrow$ ^{8}Be(2^+) and ^{12}C(0^+) $\rightarrow$ ^{8}Be(2^+) involve different angular correlations. In Ref. [17] this effect was studied and conclusions were drawn for the different energy bins in ^{12}C.

The purpose of the present article is to perform a combined analysis of the two data sets with the aim of exploring the 0^+ and 2^+ composition of the broad structures seen in these two β decays. The 3α sum spectra are analyzed within the R-matrix framework, taking into account what we have learned from the angular correlations in Ref. [17]. The R-matrix framework is needed to incorporate interfering states and several decay channels in a formalism generalized to broad intermediate states. An R-matrix analysis of ^{12}B and ^{12}N β-decay spectra was presented in Refs. [2] and [7]. The data used there included only breakup via the ^{8}Be ground state and were well described by the interference of the Hoyle state and a 0^+ state at 11–12 MeV. A 2^+ state above the 1^+ peak was included to reproduce the high-energy part of the ^{12}N spectrum. Owing to an energy cutoff, these data did not include the Hoyle peak, and when extrapolating the fit to this energy region we now see that it is inconsistent with our new data. Therefore the present work extends the analysis in Ref. [2] in two ways: The data include the Hoyle state and the analysis takes into account breakup via higher energies in ^{8}Be. The level of statistics is also significantly higher in the present data.

A description of the two experiments and measured data follows next. In Sec. IV the R-matrix formalism for multiple levels and many channels including decay via broad interme-

diate states is introduced. The analysis of the data is presented in Sec. VI in steps of increasingly complex models fitted to the data. Finally, the results are discussed and summarized.

II. EXPERIMENTS

A brief description of the two experiments is given here. Detailed explanations are published elsewhere. The first experiment utilized the IGISOL facility at the Jyväskylä Accelerator Laboratory (JYFL), Jyväskylä, Finland [15–18]. The experimental details for these measurements are given in Refs. [15–17]. Beams of ^{12}N and ^{12}B were produced, accelerated to about 25 keV, and mass separated using the ISOL method before reaching the experimental setup. A thin carbon foil was used to stop the nuclei in which they subsequently β decayed to ^{12}C, and if excited states were populated, they would break up to 3α particles or de-excite via γ-ray emission. A setup of three segmented detectors with a large solid-angle coverage detected the α particles and an HPGe detector was added to the setup to detect γ rays emitted in decays of the 4.44-MeV state in ^{12}C used for absolute normalization.

The second measurement of the β-delayed 3α breakups was carried out at the Kernfysisch Versneller Instituut (KVI), Groningen, The Netherlands. (See Refs. [15] and [19] for details). High-energy beams of ^{12}N and ^{12}B were produced and separated in the TriμP separator, after which they were defocused and implanted in a very finely segmented detector. The β decay and subsequent 3α breakup took place inside this detector, and the total 3α energy was detected, plus a small amount of energy deposited by the β particle before it escaped the detector.

III. DATA

In this work the 3α sum spectra from the two experiments are analyzed. JYFL spectra were constructed by adding the 3α-particle energies. The spectra are separated into two parts corresponding to breakup via the ^{8}Be ground-state peak at 0.0918 MeV above the 2α threshold (see Figs. 1 and 3) and breakup via excited states (all breakups that do not proceed via the ground-state peak). Contributions to the excited-state spectra are breakups via the ground-state "ghost" and via 2^+ states (see Sec. IV). The detection efficiency depends on the breakup kinematics and has been calculated for each of the two channels [17,20]. The resulting spectra were normalized using the data from the Ge detector (see Ref. [16] for details) and are shown in Fig. 2.

The 3α sum spectra were detected directly in the KVI experiment and the number of implantations gave the absolute scale. The KVI spectra shown in Fig. 2 provide better statistics than the JYFL data and provide data to low energies including the Hoyle peak.

The 12.71-MeV peaks are seen to have different shapes in the KVI and JYFL spectra. The JYFL peak is broader and has a low-energy tail. This is caused by events where the energy losses in the foil and detector dead layers are not fully
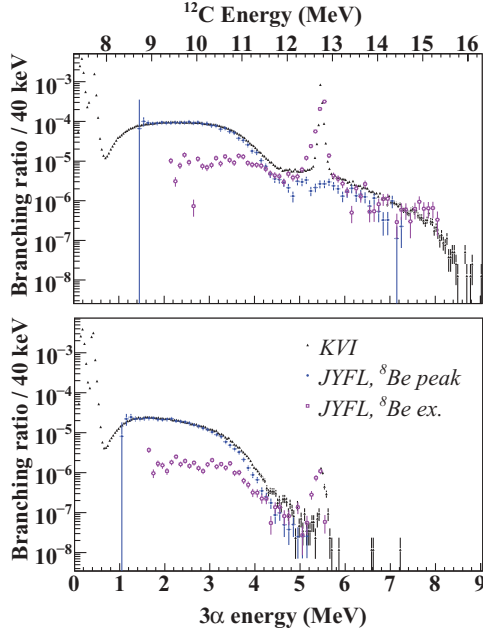
FIG. 2. (Color online) 3α energy spectra for ^{12}N decay (top) and ^{12}B decay (bottom). JYFL spectra are separated into spectra for decay via the ^{8}Be ground-state peak (filled circles) and via ^{8}Be excited states (open squares) and differ from the spectra in Fig. 1 in Ref. [15] owing to the coarser binning used here.

corrected for. Note, however, that the areas under the two peaks are consistent with each other [15].

The KVI spectra are shifted to higher energy by up to 50 keV compared to the JYFL data, owing to the small energy deposited by the β particle. The low-energy peak below the Hoyle peak in Fig. 2 is energy deposited by β particles from decays to bound states. A simulation of the energy-dependent β response was performed and was used to correct the calculated fit spectra.

IV. R-MATRIX FORMALISM

The β-delayed triple-α breakup is treated using R-matrix formalism [21] as the succession of two two-body disintegrations. First, the ^{12}C state breaks up to ^{8}Be and an α, followed by the $\alpha + \alpha$ breakup of ^{8}Be (see Fig. 1). Only the lowest 0^+ and 2^+ states in ^{8}Be are assumed to contribute appreciably. High-energy channels such as the proton channel with a 15.96-MeV threshold energy and the $L = 4$ channel via the 2^+ state are not included. For each of the ^{8}Be states one can use the single-level, single-channel R-matrix expression [22] for the 2α resonance shapes,

$$\rho_{j_b}(E') = \frac{P_{j_b}(E')\gamma_{j_b}^2}{\left| E'_{j_b} - E' - [S_{j_b}(E') - B_{j_b} + iP_{j_b}(E')]\gamma_{j_b}^2 \right|^2}, \tag{1}$$

where j_b is the spin of the ^{8}Be state and E' is the energy above the 2α threshold. γ_{j_b} is the reduced width of the 2α breakup channel, and B_{j_b} the boundary condition parameter. Plots of ρ_{j_b} are shown in Fig. 3. Note that the 0^+ channel also
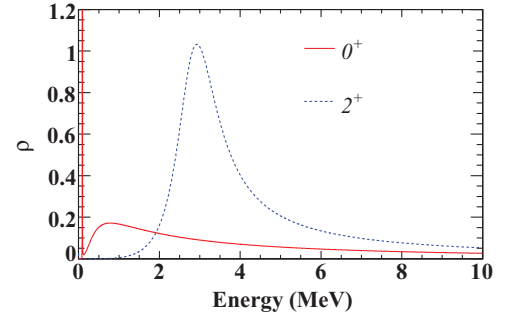

FIG. 3. (Color online) The ^{8}Be ground state and lowest 2^+ state in the single-level R-matrix model. The ground-state spectrum consists of the peak 91.8 keV above the threshold and the "ghost" at higher energy.

contributes significantly above the ground-state peak, so that both channels contribute over an extended energy region. The $\alpha + {}^8$Be breakup of states in the triple-α continuum is treated here by replacing the standard penetrabilities $P_l(E - E'_{j_b})$ and shift functions $S_l(E - E'_{j_b})$, where E'_{j_b} is the ^{8}Be-state energy, by the weighted mean values,

$$\mathcal{P}_{j_b l}(E) = \int_0^{E_{\max}^{j_b}} P_l(E - E')\rho_{j_b}(E')/\pi \, dE', \tag{2}$$

and a similar expression for the shift function $\mathcal{S}_{j_b l}$. $E_{\max}^{j_b}$ is the upper integration limit for the ^{8}Be state, chosen so that the 0_1^+ and 2_1^+ states are the dominating states in their respective integration intervals. We do not choose infinity as the upper limit, because other 0^+ and 2^+ channels contribute at higher energy. Our normalization in Eq. (2) corresponds to the formula in Ref. [26]. In the literature a different normalization has been suggested [23]:

$$\mathcal{P}_{j_b l}(E) = \frac{\int_0^{E_{\max}^{j_b}} P_l(E - E')\rho_{j_b}(E')dE'}{\int_0^{E_{\max}^{j_b}} \rho_{j_b}(E')dE'} \tag{3}$$

(with $E_{\max}^{j_b} = \infty$ in Ref. [23]), which differs for the 0^+ channel by about 30% with our choice of $E_{\max}^{j_b}$. Effectively this corresponds to a renormalization of the reduced widths for the ^{12}C states [see Eq. (7)]. The convergence of the numerator of Eq. (3) is much faster than the convergence of the denominator, so Eq. (2) is less dependent on the choice of integration limits than Eq. (3) is. It can be shown analytically that $\int_0^\infty \rho_{j_b}(E')dE' = \pi$ for all unbound states, independent of the width and energy, so for $E_{\max}^{j_b} = \infty$, Eqs. (2) and (3) are identical. The approximation used for narrow states in Ref. [22], $\int_0^\infty \rho_{j_b}(E')dE' = \pi/[1 + \gamma_{j_b}^2 dS/dE|_{E_{j_b}}]$, is only correct if the integration is restricted to the peak energy region. Taking the ^{8}Be ground state as an example, the peak area can be calculated to 0.57π using the narrow state approximation, but this is not the full integral of ρ_{j_b} because the high-energy tail or "ghost" [27] of the state contributes at higher energy (see Fig. 3), giving a total integral of π.

The β-decay probability to ^{12}C states with spin j_a above the 3α threshold is now

$$W_{j_b l}^{j_a}(E) = c^2 f_\beta \mathcal{P}_{j_b l}(E) \left| \sum_{\lambda \mu} g_{\lambda,\mathrm{GT}}^{j_a} \gamma_{\mu j_b l}^{j_a} A_{\lambda \mu}^{j_a}(E) \right|^2, \qquad (4)$$

where $g_{\lambda,\mathrm{GT}}^{j_a}$ is the β-strength parameter for Gamow-Teller transitions. The level matrix, A, is defined by its inverse,

$$A_{\lambda \mu}^{j_a}(E)^{-1} = \left(E_\lambda^{j_a} - E \right) \delta_{\lambda \mu} - \sum_{j_b l} \gamma_{\lambda j_b l}^{j_a} \gamma_{\mu j_b l}^{j_a}$$

$$\times \left[\mathcal{S}_{j_b l}(E) - \mathcal{B}_{j_b l}^{j_a} + i \mathcal{P}_{j_b l}(E) \right]. \qquad (5)$$

The boundary conditions $\mathcal{B}_{j_b l}^{j_a}$ for the interfering ^{12}C states with spin-parity j_a^+ are the shift functions $\mathcal{S}_{j_b l}(E_B^{j_a})$ evaluated at the chosen boundary energy $E_B^{j_a}$. If one chooses a resonance energy $E_\lambda^{j_a}$ as the boundary energy, the resulting fit parameters, $E_\lambda^{j_a}$, $\gamma_{\lambda j_b l}^{j_a}$, and $g_{\lambda,\mathrm{GT}}^{j_a}$, for the resonance λ will be the "observable" resonance energy, reduced widths, and β strength, respectively. For other resonances, μ, with spin-parity j_a^+, the "observables" are found by transforming the parameters to a set of parameters corresponding to the alternative boundary conditions $\mathcal{B}_{j_b l}^{j_a} = \mathcal{S}_{j_b l}(E_\mu^{j_a})$ [24].

An alternative $\tilde{A}^{-1}$ [25] can be calculated from the observable parameters, $\tilde{E}_\lambda^{j_a}$, $\tilde{g}_{\lambda,\mathrm{GT}}^{j_a}$, and $\tilde{\gamma}_{\lambda j_b l}^{j_a}$, without the need for boundary conditions, $\mathcal{B}_{j_b l}^{j_a}$,

$$\tilde{A}_{\lambda \mu}^{j_a}(E)^{-1}$$
$$= \left(\tilde{E}_\lambda^{j_a} - E \right) \delta_{\lambda \mu} - \sum_{j_b l} \tilde{\gamma}_{\lambda j_b l}^{j_a} \tilde{\gamma}_{\mu j_b l}^{j_a} [\mathcal{S}_{j_b l}(E) + i \mathcal{P}_{j_b l}(E)]$$
$$+ \sum_{j_b l} \begin{cases} \left(\tilde{\gamma}_{\lambda j_b l}^{j_a} \right)^2 \mathcal{S}_{j_b l}\left(\tilde{E}_\lambda^{j_a} \right), & \lambda = \mu, \\ \tilde{\gamma}_{\lambda j_b l}^{j_a} \tilde{\gamma}_{\mu j_b l}^{j_a} \dfrac{\left(\mathcal{S}_{j_b l}\left(\tilde{E}_\lambda^{j_a} \right)\left(E - \tilde{E}_\mu^{j_a} \right) - \mathcal{S}_{j_b l}\left(\tilde{E}_\mu^{j_a} \right)\left(E - \tilde{E}_\lambda^{j_a} \right) \right)}{\tilde{E}_\lambda^{j_a} - \tilde{E}_\mu^{j_a}}, & \lambda \neq \mu. \end{cases}$$
$$(6)$$

The corresponding decay probability is the same as Eq. (4), but with $g_{\lambda,\mathrm{GT}}^{j_a} \gamma_{\mu j_b l}^{j_a} A_{\lambda \mu}^{j_a}(E)$ replaced by $\tilde{g}_{\lambda,\mathrm{GT}}^{j_a} \tilde{\gamma}_{\mu j_b l}^{j_a} \tilde{A}_{\lambda \mu}^{j_a}(E)$.

The treatment of the three-body breakup as a sequential decay is an approximation that can only be justified when the intermediate state is long-lived; see the discussion in Sec. XIII 2 of Ref. [26]. We employ the formalism also for broad intermediate states where it is not possible to separate the different decay channels cleanly, and we must therefore consider what effects this may have (the possibility of nonresonant breakup is discussed in Sec. VII). One obvious shortcoming is the lack of symmetrization of the final states that consist of three identical bosons. This affects the R-matrix expression for breakup via excited states in ^{8}Be, as we do not know the order of emission of the 3α particles [28]. It has been shown that symmetrization affects the single-α spectrum for the breakup of the ^{12}C 1^+ state at 12.7 MeV [11], but it is assumed to be less significant in the 3α sum spectrum. In the angular correlations analysis presented in Ref. [17] the R-matrix expressions are fully symmetrized.

When calculating the decay probability it would be more correct to use $W_{j_b l}^{j_a}(E) = \int_0^\infty W_{j_b l}^{j_a}(E, E') \rho_{j_b}(E') dE'$, but this is not computationally feasible. The advantage of using the integrals $\mathcal{P}_{j_b l}(E)$ and $\mathcal{S}_{j_b l}(E)$ is that they are independent of the ^{12}C-state parameters, so only the boundary conditions $\mathcal{B}_{j_b l}^{j_a}$ have to be calculated when $E_\lambda^{j_a}$ is changed.

The R-matrix formalism used in this work is the alternative form without boundary conditions [Eq. (6)] [25]. The advantage of this is that the observables are obtained directly from the fit. This requires more computations compared to the standard formalism, however, as the shift functions $\mathcal{S}_{j_b l}(\tilde{E}_\lambda^{j_a})$ must be updated each time the resonance energy changes, whereas the boundary conditions can be kept fixed in the standard formalism. The two parametrizations have been tested in a fit to the 2α breakup of ^{8}Be to give consistent results. When applied to the 3α breakup considered here, the results are similar, but not identical, providing us with a measure of the uncertainty of the approximated shift functions and penetrabilities. It is shown in Sec. VI that this is only a minor approximation, by comparing fit results for the two parametrizations.

V. IMPLEMENTATION

The minimization tool used in this work is the Minuit2 package [29] implemented within the ROOT framework [30]. The function to minimize is the sum of a log likelihood function for the KVI data and a least-squares minimization for the efficiency-corrected JYFL data, as the JYFL data are not Poisson distributed after efficiency correction. The 1^+ peak at 12.71 MeV is excluded and the upper fit limit is just below the 15.11-MeV peak. The 12.71-MeV state is very narrow and it can be shown that the tails of its line profile do not affect the fit. The Hoyle peak is included with its area only, as its shape is strongly affected by the β response. The area is calculated using the single-level, narrow-state approximation of Eq. (4). The width and energy of the Hoyle state are kept fixed at $\Gamma_H = 7.65 \times 10^{-6}$ MeV[1] and $E_H = S_{3\alpha} + 0.3794$ MeV [1], respectively.

The R-matrix parameters for the ^{8}Be ground state are found from the energy and observed width tabulated in Ref. [33]. The 2^+ excited-state parameters are from Ref. [34] (Table II, column 3). The channel radius used is 4.5 fm. Using these parameters the resonance forms ρ_{j_b} shown in Fig. 3 are calculated. For the 0^+ state $E_{\max}^0 = 5$ MeV and for the 2^+ state $E_{\max}^2 = 10$ MeV in this work.

The small amount of energy deposited by the electrons and positrons in the detector in the KVI experiment is accounted for by folding the calculated spectra with the simulated β-response function before comparison to the KVI spectra. This has to be done at each step in the fitting routine before calculating χ^2. The uncertainty of the simulated β response is not taken into account, but in a reasonable assumption it is energy

---

[1]Note that this value differs from the value cited in Ref. [1] and is found from the values of Γ_π / Γ and Γ_π in Refs. [31] and [32], respectively.

independent, and the effect of this neglect is only to weight the KVI data slightly more highly than appropriate in the fit.

The number of free parameters in the fit depends on the number of states and breakup channels. For each state there are a level energy, E_λ; β strengths, $g_\lambda(^{12}N/^{12}B)$; and a reduced width for each breakup channel, $\gamma_{\lambda j_b l}$. There are two breakup channels for 0^+ states in ^{12}C: $l = 0$, $j_b = 0$, and $l = 2$, $j_b = 2$. For the 2^+ states there are four possibilities: For $j_b = 0$ the angular momentum can only be $l = 2$; for $j_b = 2$ it can be $l = 0, 2, 4$. The $l = 4$ channel is not considered in this work. It would contribute appreciably only at the very high-energy end of the ^{12}N spectrum (see Ref. [17]). Thus five additional free parameters are added for each 0^+ state, and six for each 2^+ state. The channel radius is kept fixed in the fit at a value common for all states, $a = r_0(A_1^{1/3} + A_2^{1/3})$. A first choice for r_0 is 1.71 fm, as in Ref. [20]. This is a large value compared to typical applications of R-matrix theory but is physically motivated by the large extension of the Hoyle state. The r_0 parameter can be considered a free parameter to be minimized in the fit, but care should be taken when going to large radii. The effects of varying the channel radius are discussed in Sec. VI.

VI. ANALYSIS

The analysis proceeds by looking at increasingly more complex models of the triple-α continuum. The starting point is what we already know has to be there: The Hoyle state at 7.654 MeV in ^{12}C or just 0.3794 MeV above the 3α threshold. We also know, from a separate analysis of the JYFL data [17], that the broad components in the spectra arise from some combination of 0^+ and 2^+ states and are dominated by 0^+ below the 12.71-MeV peak and by 2^+ above it. The existence of additional 1^+ states is ruled out in Ref. [17], which is as expected, as a 1^+ state would be narrow [35]. The models to consider are therefore combinations of 0^+ and 2^+ states, with the 0^+ Hoyle state as the lowest energy level in all models. Before proceeding to the fits, let us consider what is expected from a model fitting the data just by looking at the spectra. The KVI spectra in Fig. 2 here are shown in Fig. 2 of Ref. [15] corrected for β-phase space. The broad structures are seen here to have increasing strength as the energy increases. The component below the 12.71-MeV peak has its maximum at 10.5 MeV, and it is evident that something more than the Hoyle state is needed to produce this structure. Above the peak the strength in the ^{12}N spectrum steadily increases all the way up to the Q value. One would expect at least one resonance in this region or at higher energy.

In Table I the nine different combinations (Models 1–9) considered in the present analysis are listed. Each of these is discussed here.

(i) *The Hoyle state.* In Model 1, only the Hoyle state is included in the fit. We already know that all models with only 0^+ states can be excluded [17], but the simplest cases are considered, nonetheless, to illustrate their properties. The fit spectra are shown in Fig. 4 for ^{12}N and ^{12}B β decay, respectively. The only feature of the spectra that is reproduced is the narrow Hoyle

TABLE I. Applied *R*-matrix models (different combinations of 0^+ and 2^+ states) and their reduced χ^2 values. The number of degrees of freedom (df) is 1251 minus the number of free parameters (see Sec. V).

Model	χ^2/df	r_0 (fm)	Fig. no.(s.)
1: 0^+	281	1.71	4,5
2: $0^+, 0^+$	15.9	1.71	4,5
3: $0^+, 2^+$	44.8	1.71	4,5
4: $0^+, 0^+, 0^+$	3.24	1.71	4,5
5: $0^+, 0^+, 2^+$	6.06	2.09	4,5
6: $0^+, 2^+, 2^+$	18.4	1.71	4,5
7: $0^+, 0^+, 0^+, 2^+$	1.24	2.47	6
8: $0^+, 0^+, 2^+, 2^+$	1.65	2.47	7
9: $0^+, 0^+, 0^+, 2^+, 2^+$	1.21	2.47	8

peak just above threshold. The small increase in the calculated spectrum just above the peak (the "ghost" of the Hoyle state [27]) is similar in shape to the measured spectrum in this energy region, which explains part of the structure. Looking at the value of χ^2/df = 281 in Table I, it is much larger than unity, as expected. The spectra for decay through the ^8Be ground-state peak and excited states are separated in Fig. 5. Only breakup via the ground state contributes, owing to the low energy of the Hoyle state. The component for decay via excited energies arises owing to the ^8Be ground-state "ghost" shown in Fig. 3.

(ii) *The Hoyle state plus one additional state.* The next step is the addition of a 0^+ state (Model 2). The resulting χ^2 is still much larger than the number of degrees of freedom (df), but it is a large improvement
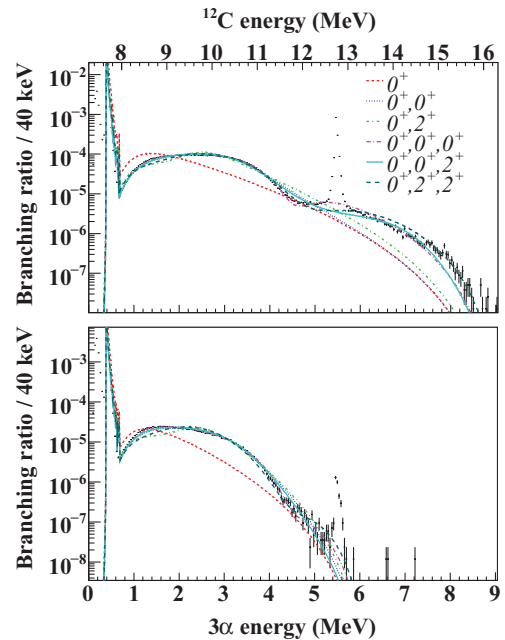

FIG. 4. (Color online) 3α energy spectra from the KVI experiment for ^{12}N (top) and ^{12}B (bottom) decay. Fits to Models 1 to 6 in Table I are shown.

FIG. 5. (Color online) ^{12}N decay spectra from the JYFL experiment. 3α energy spectra for the ^{8}Be ground-state peak (top) and excited-state (bottom) channels are shown. The excited-state channels are the ^{8}Be ground-state "ghost" and the 2^+ contribution. Fits to Models 1 to 6 in Table I are shown.

FIG. 6. (Color online) Fit to Model 7 in Table I (three 0^+ and one 2^+ states). Only ^{12}N spectra are shown. The KVI 3α energy spectra are shown in both plots, compared to the solid line showing the total fit spectrum summed over all channels. JYFL 3α energy spectra for the ^{8}Be peak (top) and excited-state (bottom) channels are compared to the dashed curves, which are the fit components for the respective channels. The dotted and dot-dashed lines are contributions to each decay channel from the 0^+ and 2^+ states in ^{12}C, respectively.

from Model 1. It is interesting to note that the energy region from 1 to 4 MeV is adequately described in Figs. 4 and 5. For the ^{12}B case, with the smaller β-decay energy window, this model is sufficient and shows that 0^+ interference is an important ingredient for the understanding of the spectrum in this region.

In Model 3 we are replacing the upper 0^+ state by a 2^+ state, which worsens the fit several times. It was shown in Ref. [17] that a 2^+ contribution is needed, but this analysis shows that it is apparently not a single state above the Hoyle state.

(iii) *The Hoyle state plus two additional states.* Models 4 and 5 show that the addition of a 0^+ or a 2^+ state to Model 2 gives an improvement in χ^2 of a factor of almost 5. Model 6 with two 2^+ states above the Hoyle state fails to do this, and the χ^2 values fall in between the results for Models 2 and 3. Model 6 also fails in describing the flat region at 8.8- to 10.5-MeV excitation energy as shown in Fig. 4. Also, the upper 2^+-state energy and β strengths go to their upper limits.

The fit with three 0^+ states (Model 4) is the best fit so far. The only visible discrepancy in the spectra is a dip below the measured spectra at 11.8 MeV. Model 5 fails at describing the data from breakup via the ^{8}Be ground state and also has problems in areas where the KVI spectra change rapidly (at 8.5 and 11–12 MeV.)

(iv) *The Hoyle state plus three additional states.* At this point it seems clear that the addition of at least one more state is needed to describe the data. Here we can right away exclude four 0^+ states, because of the missing 2^+ component. Also, three 2^+ states above the Hoyle state

can be ruled out because the Hoyle state is not sufficient as the dominating broad 0^+ component below the 1^+ peak. This leaves us with Models 7 and 8 in Table I. Figures 6 and 7 show the fits found to these two models. Both reproduce the spectra very well except for a small systematic deviation at high energy in the ^{8}Be peak channel. The χ^2 value reveals that three 0^+ and one 2^+ states is in fact the better model, with $\chi^2/\mathrm{df} = 1.24$ compared to $\chi^2/\mathrm{df} = 1.65$. We cannot argue for a more complex model from the data used in the fit, as the R-matrix model used is only an approximation and the uncertainty in the β response is not taken into account, so an improvement in reduced χ^2 of 0.2 would be comparable to the systematic uncertainty. However, both models are inconsistent with the results from angular correlations in the JYFL data [17], as the ^{8}Be excited-state spectrum both below and above the 1^+ peak is dominated by 0^+ in Fig. 6 and 2^+ in Fig. 7.

(v) *The Hoyle state plus four additional states.* The models with four unbound states are therefore insufficient. We will not proceed by testing all models with five unbound states, as the parameter space becomes very large, but Model 9 in Table I illustrates that, if we include the upper 2^+ state from Model 8 in the best fit so far (Model 7), we obtain a spectrum (Fig. 8) that is consistent with both the datum spectra in the fit and also the angular correlation analysis.
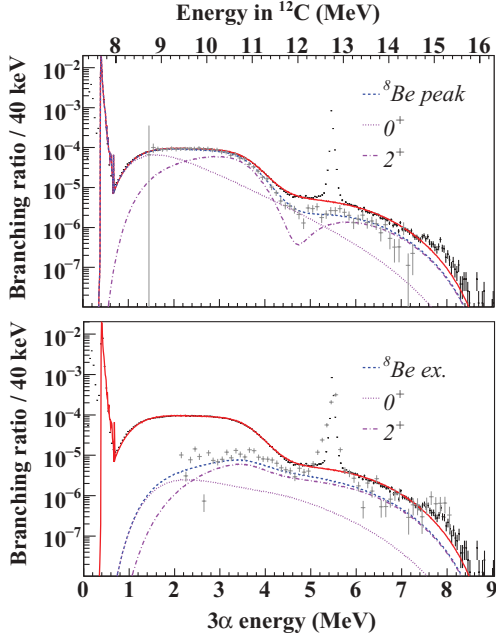
FIG. 7. (Color online) Fit to Model 8 in Table I (two 0^+ and two 2^+ states). See Fig. 6 caption for explanation.

The r_0 parameters used in the fits are shown in Table I. For the simple models the value $r_0 = 1.71$ fm has been used and is generally not the optimized value, as the models are easily rejected. Larger values were tested in the fit to Model 1 (Hoyle state only), but this gave a worse χ^2. For the more complex models different r_0 values have been tested, and for Models 7–9 the optimum value is $r_0 = 2.47$ fm (out of the discrete set: 1.71, 2.09, 2.47, and 2.85 fm). For Models 7 and 8 the level energies in fits to three different r_0 values are
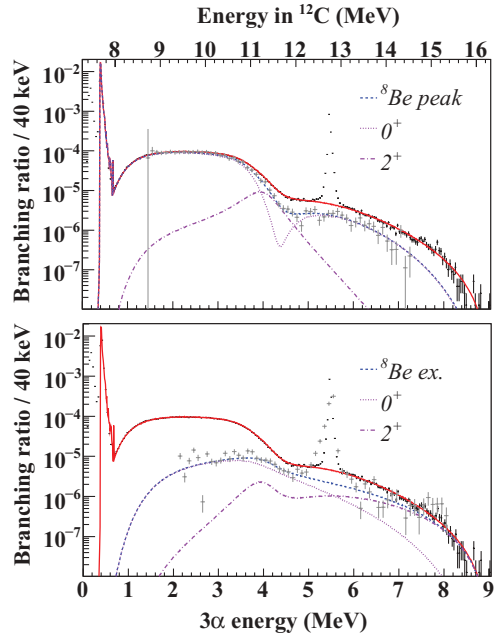
FIG. 8. (Color online) Example fit to Model 9 in Table I (three 0^+ and two 2^+ states). See Fig. 6 caption for explanation.

shown in Fig. 9. For the three lowest-energy states the results are largely independent of the channel radius, lending further support to these resonances being physical. The energy of the upper 0^+ state in Model 7 decreases with increasing r_0. This effect is known in the literature [36] and indicates that this is not a physical resonance. The physical effect responsible for this component might be the sum of contributions from several high-energy resonances or decay directly via the continuum. This is discussed in Sec. VII. The upper 0^+ state of Model 8 does not show the same monotonous decrease in energy, but this is probably because an additional 0^+ state is needed in the 10- to 11-MeV energy region and the fit is trying to compensate for this.

Properties of the resonances found in the fits are described in the following. The observables that are interesting for comparison to other work are resonance energies, E_λ; observed widths,

$$\left(\Gamma_\lambda^{j_a}\right)^o = \frac{\sum_{j_b l} 2\mathcal{P}_{j_b l}\left(\gamma_{\lambda j_b l}^{j_a}\right)^2}{1 + \sum_{j_b l}\left(\gamma_{\lambda j_b l}^{j_a}\right)^2 \left.\frac{\delta \mathcal{S}_{j_b l}}{\delta E}\right|_{E=E_\lambda^{j_a}}}; \qquad (7)$$

and $B_{\mathrm{GT},\lambda}$ values,

$$B_{\lambda,\mathrm{GT}}^{j_a} \propto \frac{\left|g_{\lambda,\mathrm{GT}}^{j_a}\right|^2}{1 + \sum_{j_b l}\left(\gamma_{\lambda j_b l}^{j_a}\right)^2 \left.\frac{\delta \mathcal{S}_{j_b l}}{\delta E}\right|_{E=E_\lambda^{j_a}}}. \qquad (8)$$

The expressions for the observed width and B_{GT} values are derived from the single-level approximation of Eq. (4) and

TABLE II. Comparison of fits using alternative (alt.) and standard (stand.) *R*-matrix parametrizations. Differences are caused by our approximate description of three-body breakup and provide a measure of the systematic uncertainty.

		Model 9		Model 7	
		Alt.	Stand.	Alt.	Stand.
0_2^+	E (MeV)	7.65	7.65	7.65	7.65
	Γ^o (eV)	7.65	7.65	7.65	7.65
	$B_{\mathrm{GT}}(^{12}\mathrm{N})$	0.090	0.090	0.090	0.090
	$B_{\mathrm{GT}}(^{12}\mathrm{B})$	0.108	0.108	0.108	0.108
0_3^+	E (MeV)	11.01	11.00	11.58	11.08
	Γ^o (MeV)	1.31	1.33	2.68	1.61
	$B_{\mathrm{GT}}(^{12}\mathrm{N})$	0.075	0.078	0.026	0.051
	$B_{\mathrm{GT}}(^{12}\mathrm{B})$	0.093	0.099	0.023	0.066
2_2^+	E (MeV)	11.3	11.4	10.8	11.4
	Γ^o (MeV)	0.87	1.44	1.77	2.06
	$B_{\mathrm{GT}}(^{12}\mathrm{N})$	0.024	0.045	0.051	0.089
	$B_{\mathrm{GT}}(^{12}\mathrm{B})$	0.027	0.046	0.071	0.097
0_4^+	E (MeV)	61.0	65.8	24.1	26.2
	Γ^o (MeV)	1109	200	154	13.2
	$B_{\mathrm{GT}}(^{12}\mathrm{N})$	53	19	53	112
	$B_{\mathrm{GT}}(^{12}\mathrm{B})$	64	22	64	127
2_3^+	E (MeV)	16.5	16.7		
	Γ^o (MeV)	0.58	0.97		
	$B_{\mathrm{GT}}(^{12}\mathrm{N})$	4.9	4.0		
	$B_{\mathrm{GT}}(^{12}\mathrm{B})$	3.7	5.6		
χ^2/df		1.21	1.22	1.24	1.24

assuming that the shift function is linear over the resonance energy range. For the broad interfering states that we observe in ^{12}C the single-level approximation is rather poor, but the first-order expansion of the shift function is valid for most resonances.

Observables from fits within the standard parametrization [Eq. (5)] are compared in Table II to values from the two best models, 7 and 9 [Eq. (6)]. Energies and χ^2 are similar in the two pairs of fits but widths and B_{GT} values differ substantially. These are the same tendencies as seen in fits within the same formalism but with different limits on the parameters or different initial parameters. This justifies approximating the shift functions and penetrabilities as weighted mean values for the broad intermediate states.

Figure 10 shows level energies in ^{12}C for the resonances in the different fit models. Owing to the "ghost" effect, the Hoyle state also contributes at energies higher than its peak. This leads to the interesting possibility of trying to measure the width of this state from the present data [20]. However, owing to the uncertainty in the contribution of other states, it is not possible at the present stage to improve on the literature value using this idea. Both energy and width are therefore kept fixed in the fit. We see this level in Fig. 10 just above the 3α threshold. The B_{GT} value for this state is given by the peak branching ratio and has already been published [15].

At higher energy we find a 0^+ and 2^+ state in the energy region below the 12.71-MeV peak. Both have energies that do not vary much in fits to different models (Fig. 10) or different r_0 values (Fig. 9). The widths and B_{GT} values differ, however, by at least a factor of 2 in different fits, but we know that the states are broad. Recommended observable values for these states are given in Table III. The values and errors are found by comparing results from fits to Models 7–9 (except Model 8 for the 0_3^+ state) and fits for different r_0 values.

The next resonance in the fits is a 2^+ state with energy varying somewhat more than the low-energy 0^+ and 2^+ states but remaining close to the ^{12}N Q value. Its width and B_{GT} values cannot be determined.

The upper 0^+ state has an energy above the Q value, but otherwise it cannot be determined. The reduced widths and β strengths often go to the upper limits allowed in the fit so the
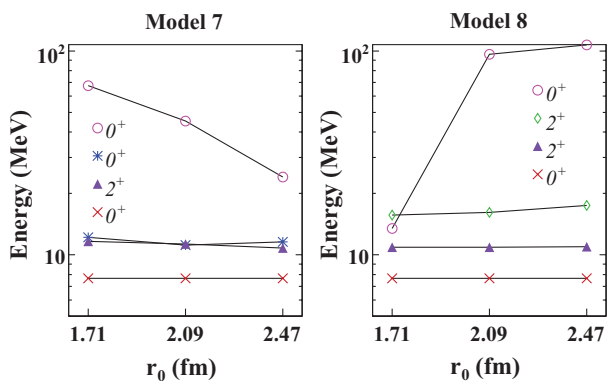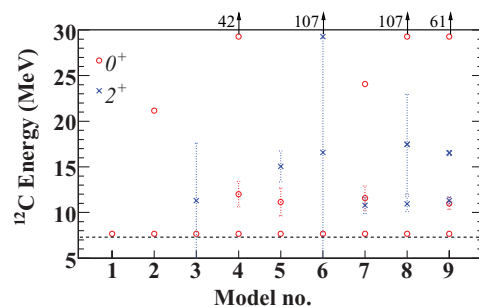

FIG. 10. Level energies for the fits in Table I. Note the systematic uncertainty in the extracted energies (see text). Dotted lines are not error bars but indicate observed widths. For clarity these are omitted for the upper 0^+ states, which have extremely large widths. The triple-α threshold is indicated by the dashed horizontal line.

width and B_{GT} values cannot be determined; we can only see that they have to be very large.

VII. DISCUSSION

More details regarding the low-lying resonance structure of ^{12}C are seen in the present data and analysis compared to those presented in Refs. [2] and [7], owing to better statistics combined with information about decay channels from the JYFL data. Model 5 in Table I was found to fit the data in Refs. [2] and [7], with a 0_3^+ state at 11.5 MeV and a 2_3^+ state at 13.6 MeV. A more complex model is needed to describe the new data, not because the data sets are inconsistent, but mainly because of the extension of the data range to low energy and the inclusion of more complex breakup channels via higher energies in ^{8}Be.

It is difficult to compare our results directly to what has been measured in other experiments. Because of the combination of very broad structures in the spectra and decay via broad intermediate states, the complete treatment in the R-matrix formalism yields spectra that cannot be separated into contributions from the individual states of a certain spin-parity owing to the effects of interference, and maxima in the spectra do not necessarily correspond to a resonance energy. Another important difference is that the relative feeding to states in β decay will differ from what is observed in reaction or scattering experiments. Bearing this in mind we now discuss

FIG. 9. (Color online) Level energies in R-matrix fits to different channel radii. Note the systematic uncertainty in the extracted energies (see text).

TABLE III. Recommended observable values for the 0_3^+ and 2_2^+ states from this work.

		Recommended value
0_3^+	E (MeV)	11.2 ± 0.3
	Γ^o (MeV)	1.5 ± 0.6
	$B_{GT}(^{12}$N)	0.06 ± 0.02
	$B_{GT}(^{12}$B)	0.07 ± 0.03
2_2^+	E (MeV)	11.1 ± 0.3
	Γ^o (MeV)	1.4 ± 0.4
	$B_{GT}(^{12}$N)	0.05 ± 0.03
	$B_{GT}(^{12}$B)	0.06 ± 0.04

our results in comparison to other work, both experiments and theory.

Beginning with the 0_3^+ state, the position is consistent with the β-decay results presented in Refs. [2] and [7]. The resonance energy of this state is larger than the 10.3 MeV tabulated in Ref. [1], and does not coincide with a peak in the spectra, but the interference between the 0^+ states gives the very broad component from 8.5 to 11 MeV, which has been mistaken for a 10.3-MeV resonance with a 3-MeV width. A 0^+ strength is also seen to dominate in the spectra from 8 to 12 MeV in inelastic α [3] and proton [4] scattering on ^{12}C.

A lot of effort has been put into the search for a 2^+ rotational excitation of the Hoyle state, but its existence and resonance energy have yet to be determined unambiguously by experiment. If this state can be found, it might reveal structural properties of the Hoyle state, as discussed in Ref. [4], and depending on its energy, it could contribute to the triple-α reaction at high temperatures [4,7]. In this work we argue for the existence of a 2^+ state between 10.5 and 12 MeV in ^{12}C. Other reported 2^+ states in this energy region are at 11.16 MeV [1,5] and 11.46 MeV ($\Gamma^o = 0.43$ MeV [6]). Other experiments report 2^+ states below this energy region, at 9.6(1) MeV ($\Gamma^o = 600$ keV [4]) and 9.9(3) MeV ($\Gamma^o = 1.0(3)$ MeV [3]).

The coexistence of a 2_2^+ and a 0_3^+ state in the 9- to 12-MeV energy region is supported by calculations in antisymmetrized molecular dynamics (AMD) [10] and the complex-scaling method [37]. The high energy of our 0_3^+ state is also consistent with the 11.3 MeV, $\Gamma^o = 1$ MeV, 0^+ state reproduced in 3α cluster calculations [38]. Both the 0_3^+ and the 2_2^+ states are very broad, indicating a high degree of clustering in these states.

Going to the higher-energy contributions there is an experimental 2^+ candidate at 15.4 MeV, $\Gamma^o = 1.5$ MeV [1], and a well-known narrow $T = 1, 2^+$ state at 16.1 MeV, $\Gamma^o = 5.3$ keV. A 2^+ state in the 15- to 16-MeV energy region is found in no-core shell-model calculations [15]. A 2_3^+ state is also found in AMD calculations at roughly 13 MeV.

For the high-energy 0^+ contribution there are no experimental candidates. It is evident from the fits that this is not a physical resonance: But then what is its physical interpretation? There are two possibilities: Either this component in the fit tries to account for a whole range of 0^+ resonances above the data range or it is the contribution from nonresonant decay. Normally nonresonant decay is not treated with *R*-matrix formalism, but it is possible as noted in Ref. [26] (Sec. II 4, p. 265): "The only factor in *R*-matrix theory that could possibly correspond to direct mechanisms are the sums over the far-away levels." We have tested the direct-decay hypothesis by replacing the high 0^+ level with a series of square well levels ([26], Sec. IV 3), reducing the number of fit parameters to a constant energy term adding to the level energies and a common β strength to all levels. This model is seen to reproduce the spectra well, supporting the direct decay hypothesis. This question will be explored further in a forthcoming publication.

The $B_{\rm GT}$ values for the broad states complement the results given for narrow states in [15]. The strength of the 2^+ state near 16 MeV was estimated in Ref. [15] by summing the branching ratios over the 15- to 16-MeV region and using a narrow level

formula for the $B_{\rm GT}$ value. The value resulting from the *R*-matrix analysis presented here is significantly larger because the center of the level is placed at higher energy and only the tail is visible in the observed spectra. The 2^+ state found in this energy region in the no-core shell model has a large $B_{\rm GT}$ value [15]. For the 2_2^+ and 0_3^+ states found in AMD calculations in the 9- to 12-MeV energy region, the latter has a $B_{\rm GT}$ value consistent with the data, while the former is predicted with much less feeding. No 2^+ state is found with a large $B_{\rm GT}$ value in the AMD calculations.

VIII. CONCLUSION

This article marks the culmination of a series of works aimed at a better understanding of ^{12}C resonances through β-decay studies. Compared to the work done in the 1950s and 1960s, we now have much better experimental information on the population and decay of the continuum in ^{12}C fed in the β decays of ^{12}B and ^{12}N.

The picture emerging from these new high-quality data is a complex one, with the triple-α sum spectra consisting of broad structures without clearly identifiable peaks. The β-decay selection rules restrict these broad structures to spin-parity 0^+ and 2^+, and to further disentangle the 0^+ and 2^+ contributions we employ an extensive *R*-matrix framework generalized to three-body breakup via broad intermediate states including multiple levels and many channels, though not symmetrized in the order of emission of the α particles. Additional spin information comes from analysis of the breakup into 3α particles also analyzed in an *R*-matrix formalism [17]. This analysis framework can be improved only by dedicated theoreticaly work.

The result of this analysis is that one 0^+ and one 2^+ state above the Hoyle state are not enough to reproduce the spectra. Our fits give evidence of one broad 0^+ and 2^+ state in the 10.5- to 12-MeV energy region. Above the 12.7-MeV peak the β strength increases (Fig. 2 in Ref. [15]), and this is probably caused by additional 0^+ and 2^+ components at high energy.

The $B_{\rm GT}$ values for the broad states reported here complete the results for narrow states already published [15,16]. These $B_{\rm GT}$ values will provide a sensitive test of future microscopic calculations of ^{12}C.

The work presented here clearly demonstrates that a full understanding of the broad resonances in ^{12}C a few megaelectronvolts above the triple-α threshold requires an analysis framework that takes into account interference of overlapping levels as well as contributions from several decay channels. Not until data from other experimental probes giving evidence of 0^+ and 2^+ states are analyzed with this level of detail can a clear and consistent picture be expected to emerge.

[1] F. Ajzenberg-Selove, Nucl. Phys. **A506**, 1 (1990).

[2] C. Aa. Diget *et al.*, Nucl. Phys. **A760**, 3 (2005).

[3] M. Itoh *et al.*, Nucl. Phys. **A738**, 268 (2004).

[4] M. Freer *et al.*, Phys. Rev. C **80**, 041303(R) (2009).

[5] M. Freer *et al.*, Phys. Rev. C **76**, 034320 (2007).

[6] B. John, Y. Tokimoto, Y. W. Lui, H. L. Clark, X. Chen, and D. L. Youngblood, Phys. Rev. C **68**, 014305 (2003).

[7] H. O. U. Fynbo *et al.*, Nature **433**, 136 (2005).

[8] H. Morinaga, Phys. Rev.**101**, 254 (1956).

[9] H. Morinaga, Phys. Lett. **21**, 78 (1966).

[10] Y. Kanada En'yo, Prog. Theor. Phys. **117**, 655 (2007).

[11] H. O. U. Fynbo *et al.*, Phys. Rev. Lett. **91**, 082502 (2003).

[12] C. W. Cook, W. A. Fowler, C. C. Lauritsen, and T. Lauritsen, Phys. Rev. **111**, 567 (1958).

[13] D. H. Wilkinson, D. E. Alburger, A. Gallmann, and P. F. Donovan, Phys. Rev. **130**, 1953 (1963).

[14] D. Schwalm and B. Povh, Nucl. Phys. **89**, 401 (1966).

[15] S. Hyldegaard *et al.*, Phys. Lett. **B678**, 459 (2009).

[16] S. Hyldegaard *et al.*, Phys. Rev. C **80**, 044304 (2009).

[17] C. Aa. Diget *et al.*, Phys. Rev. C **80**, 034316 (2009).

[18] J. Äystö *et al.*, Nucl. Phys. **A693**, 477 (2001).

[19] S. G. Pedersen *et al.*, in *Proceedings, International Symposium on Nuclear Astrophysics—Nuclei in the Cosmos—IX*, PoS(NIC-IX)244 (2006).

[20] C. Aa. Diget, Ph.D. thesis, University of Aarhus, Denmark 2006. http://phys.au.dk/fileadmin/site_files/publikationer/phd/Christian_Aa_Diget.pdf.

[21] F. C. Barker and E. K. Warburton, Nucl. Phys. **A487**, 269 (1988).

[22] F. C. Barker, Nucl. Phys. **A609**, 38 (1996).

[23] L. Buchmann, E. Gete, J. C. Chow, J. D. King, and D. F. Measday, Phys. Rev. C **63**, 034303 (2001).

[24] F. C. Barker, Aust. J. Phys. **25**, 341 (1972).

[25] C. R. Brune, Phys. Rev. C **66**, 044611 (2002).

[26] A. M. Lane and R. G. Thomas, Rev. Mod. Phys. **30**, 257 (1958).

[27] F. C. Barker and P. B. Treacy, Nucl. Phys. **38**, 33 (1962).

[28] D. P. Balamuth, R. W. Zurmühle, and S. L. Tabor, Phys. Rev. C **10**, 975 (1974).

[29] http://seal.web.cern.ch/seal/MathLibs/Minuit2/html/.

[30] http://root.cern.ch/.

[31] D. E. Alburger, Phys. Rev. C **16**, 2394 (1977).

[32] H. Crannell *et al.*, Nucl. Phys. **A758**, 399 (2005).

[33] F. Ajzenberg-Selove, Nucl. Phys. **A745**, 155 (2004).

[34] M. Bhattacharya, E. G. Adelberger, and H. E. Swanson, Phys. Rev. C **73**, 055802 (2006).

[35] D. V. Fedorov, A. S. Jensen, and H. O. U. Fynbo, Nucl. Phys. **A718**, 685 (2003).

[36] E. K. Warburton, Phys. Rev. C **33**, 303 (1986).

[37] C. Kurokawa and K. Kato, Nucl. Phys. **A738**, 455 (2004).

[38] R. Álvarez-Rodríguez *et al.*, Eur. Phys. J. A **31**, 303 (2007).